Boost Converter with Improved Transfer Ratio

DV Nicolae[1)], CG Richards[1)] and JFJ van Rensburg[2)]

[1)] Tshwane University of Technology, Department of Electrical Engineering, Emalahleni Campus, Sotuh Africa
[2)] Vaal University of Technology, Faculty of Engineering & Technology, Vanderbijlpark, South Africa
danaurel@yebo.co.za; richardscg@tut.ac.za; hannesvr@vut.ac.za

***Abstract*— A variation on the classic boost topology is presented. The improved transfer ratio is obtained by storing energy in parallel inductors and releasing the energy in series. State-space analysis, signal flow graph and simulation validation are presented for a double inductor topology. This analysis is then compared with the experimental results on the same double boost topology.**

I. INTRODUCTION

The DC-DC boost converter has applications in the automotive, telecommunications, IT industries as well as in renewable energy generation via fuel cells, photovoltaic arrays and wind turbines [1-8]. The classic boost topology provides a limited boost factor. Previous studies proposed topologies such as the tapped-inductor, cascaded and interleaved boost converters [5-8] for achieving a higher boost ratio. This paper introduces another variation which provides a higher transfer ratio with the possibility of extending the control range.

To validate performances of this topology, a simple IP controller was implemented. Further work on this will consider other control methods such as fuzzy logic [11], sliding mode control [14] and others as mentioned in literature [10, 12, and 14].

II. PROPOSED MODEL

A. Modus operandi

Fig. 1 shows the proposed topology. Let's us firstly consider ideal components and all switches are simultaneously activated. When the switches are in ON state (see fig. 2), the each inductor L_k (k = 1,2,…n) is connected between V_b and ground through D_{jp} (j = 1,2,…n-1) and S_k; the indices "p" come from paralleling the inductors.

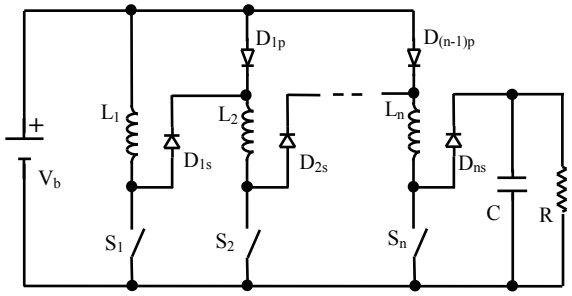

Fig. 1 Proposed Model

All the diodes D_{ks} have the anode pulled to ground through the switches and consequently they are in OFF state.

When the switches are in OFF state (see fig. 3), the back emf induced in the inductors create the condition for the "paralleling" diodes D_{jp} to be in reverse polarity and the diodes D_{ks} to be in forward polarization; the indices "s" come from series connected inductors. Hence, the inductors appear connected in series and the output voltage is going to be the sum of all voltages across the inductors plus the battery voltage.

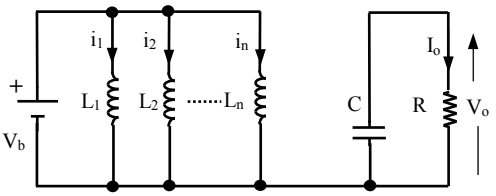

Fig. 2 ON state representation

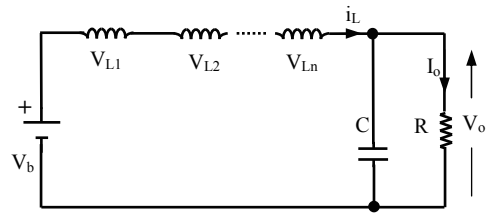

Fig. 3 OFF state representation

B. Steady-state analysis

This analysis is done assuming, in the first approximation, that all inductors are equal and with negligible resistance, the voltage drop across the diodes and switches are also negligible.

The voltage across each inductor in OFF state follows the classic theory [9]:

$$V_{Lk} = \frac{V_b}{1-\delta} - V_b \qquad (1)$$

were δ is the duty cycle.

When evaluating the output voltage for the proposed model, all the individual voltages are added together with the input voltage (fig. 4). The result can be written as:

978-1-4244-5393-1/10/$26.00 ©2010 IEEE

$$V_o = V_b + \sum_{k=1}^{n} V_{Lk} \tag{2}$$

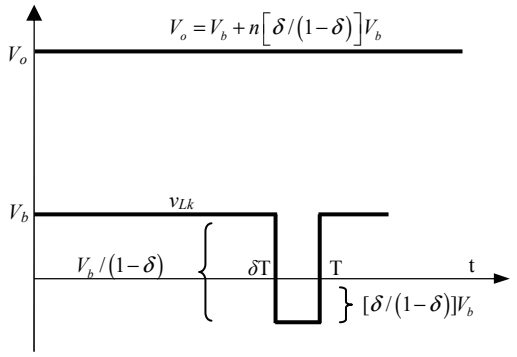

Fig. 4 Model voltages

$$V_o = V_b + n\frac{\delta}{1-\delta}V_b \tag{3}$$

From (3) results the boost factor M:

$$M = \left[1+(n-1)\delta\right]/(1-\delta) \tag{4}$$

If n =1 it is easy to find the well known boost factor of 1/(1-δ).

Taking the internal resistance of L as r_L, of the switch as r_s the voltage drop over the diode as V_d and considering the load resistance R, the boost factor is given by:

$$M = \frac{1+(n-1)\left[\delta - \dfrac{r_L+\delta r_s}{R(1-\delta)}\right]}{1-\left[\delta - \dfrac{r_L+\delta r_s}{R(1-\delta)}\right]} - \frac{nV_d}{V_b} \tag{5}$$

The quality of the diodes (volt drop) has a big influence on the transfer ratio/efficiency of the proposed topology. The rest of this paper only considers a double boost topology (n = 2).

$$M = \frac{1+\delta-(r_L+\delta r_s)/\left[R(1-\delta)\right]}{1-\delta+(r_L+\delta r_s)/\left[R(1-\delta)\right]} - \frac{2V_d}{V_b} \tag{6}$$

C. State variable analysis

Let's consider now the simplified equivalent diagram (fig. 5) for a two inductors model.

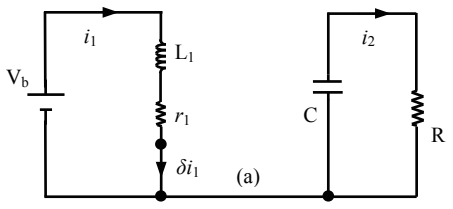

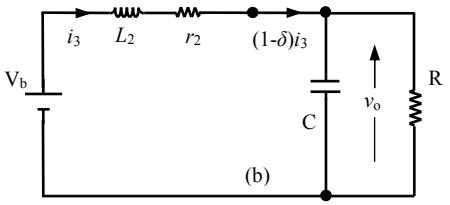

Fig. 5 Simplified equivalent circuit; a) ON state; b) OFF state

$$\begin{aligned} L_1 &= L/2 \\ r_1 &= (r_L + r_s)/2 \\ L_2 &= 2L \\ r_2 &= 2r_L \end{aligned} \tag{7}$$

The proposed boost converter can be described by its generic modes with the state space equation:

$$\dot{x} = Ax + BV_b \tag{8}$$

$$A = \begin{bmatrix} -\delta(r_L+\delta r_s)/L & 0 & 0 & 0 \\ 0 & 1/RC & 0 & 0 \\ 0 & 0 & -(1-\delta)r_L/L & 1/(2L) \\ 0 & 0 & 1/C & -1/(R^2C) \end{bmatrix} \tag{9}$$

$$B = \begin{bmatrix} 2/L \\ 0 \\ -1/L \\ 0 \end{bmatrix} \tag{10}$$

D. Signal Flow Graph analysis

Signal flow graph is another simplified version of the converter diagram [11] used to complement the analysis of the proposed boost converter. Figure 6 shows the signal flow graph of the proposed double boost converter.

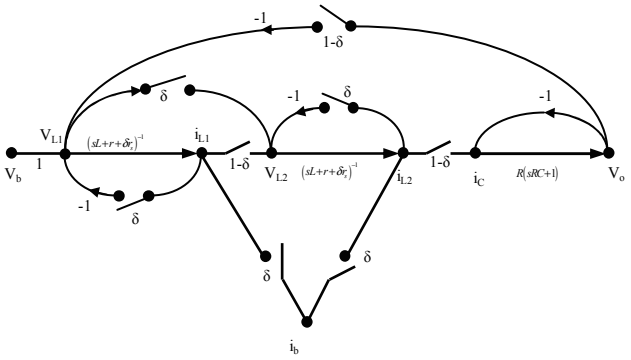

Fig. 6 Unified signal flow graph

Small-signal transfer function can be derived from this graph. The gain between v_o (s) and v_b (s) can be derived using Mason's formula:

$$\frac{v_o(s)}{v_b(s)} = \sum_k \frac{p_k \Delta_k}{\Delta} \tag{11}$$

There are two forward paths (p_1 and p_2) and five loops.

$$p_1 = \frac{(1-\delta)^2 R}{(sL + r_L + \delta r_s)^2 (sRC+1)} \tag{12}$$

$$p_2 = \frac{(1-\delta)\delta R}{(sL + r_L + \delta r_s)(sRC+1)} \tag{13}$$

$$l_1 = l_2 = \frac{-\delta}{sL + r_L + \delta r_s} \tag{14}$$

$$l_3 = \frac{-R}{(sRC+1)} \tag{15}$$

$$l_4 = \frac{-(1-\delta)^2 R}{(sL + r_L + \delta r_s)^2 (sRC+1)} \tag{16}$$

$$l_5 = \frac{-(1-\delta)^2 \delta R}{(sL + r_L + \delta r_s)(sRC+1)} \tag{17}$$

$$\frac{v_o(s)}{v_b(s)} = \frac{p_1\Delta_1 + p_2\Delta_2}{1-(l_1 + l_2 + l_3 + l_4 + l_5)} \tag{18}$$

In this graph all loops touch both forward paths:

$$\Delta_1 = \Delta_2 = 1 \tag{19}$$

Then:

$$\frac{v_o(s)}{v_b(s)} = \frac{a_1 s^1 + a_0}{b_3 s^3 + b_2 s^2 + b_1 s^1 + b_0} \tag{20}$$

$$a_1 = (1-\delta)\delta RL \tag{21}$$

$$a_0 = (1-\delta^2)R - (r_L + \delta r_s) \tag{22}$$

$$b_3 = RCL^2 \tag{23}$$

$$b_2 = (1+R)L^2 + 2LRC(1+\delta) \tag{24}$$

$$b_1 = \delta L\left[2 + R(1-\delta)\right] + RC(r_L + \delta r_s) + 2\left[(1+R)L + \delta RC\right] \tag{25}$$

$$b_0 = (1-\delta)^2 + r_L + \delta r_s \tag{26}$$

III. CONTROL SYSTEM

For this study, a simple IP controller has been used, as shown in Fig. 7.

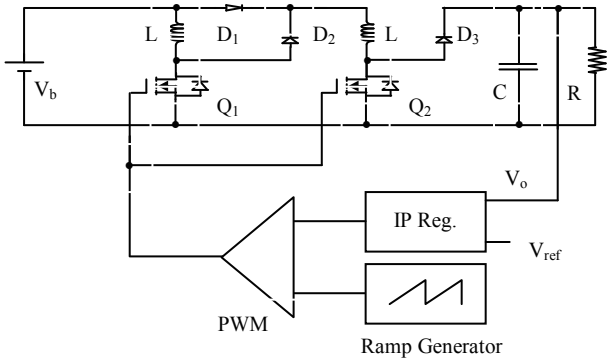

Fig.7 Double-boost converter, control system

In the steady state, the power balance between input and output can be written as:

$$V_b I_s = \frac{1}{C} \cdot \frac{d}{dt}\left(V_o^2\right) + V_o I_o \tag{27}$$

Based on this dynamic equation, majority of authors have proposed a classic PI regulator. But the closed-loop transfer function of this type of regulator has two zeros:

$$\frac{V_o^2}{V_{ref}^2} = \frac{\left(k_i + s \times k_p\right)\left(1 + s \times \tau_3\right)}{s^3 \times \left(\frac{\tau_3 C}{2}\right) + s^2 \times \frac{C}{2} + s \times k_p + k_i} \tag{28}$$

For this study an integral/proportional (Fig. 8) solution has been chosen as voltage regulator, where k_i, k_p are the integral and proportional coefficients respectively and τ_1 is the time constant of a noise-rejection low-pass filter.

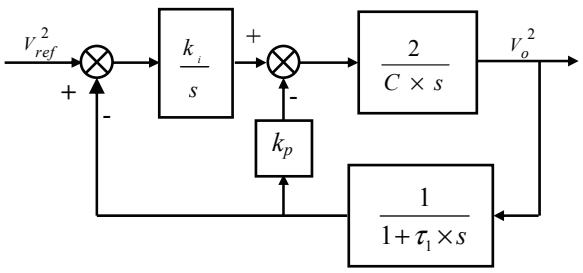

Fig. 8 IP Regulator

The close-loop transfer function of the system is:

$$\frac{V_o^2}{V_{ref}^2} = \frac{1 + s \times \tau_1}{s^3\left(\frac{\tau_1 \times C}{2k_i}\right) + s^2\left(\frac{C}{2k_i}\right) + s\left(\frac{k_p}{k_i}\right) + 1} \tag{29}$$

The equation (29) shows that the IP solution cancels a slow zero from the transfer function improving the dynamics of the regulator.

If the poles of the system (s_0, s_1 and s_2) are placed on the Butterworth circle with the radius ω_o such as: $s_o = -\omega_o$, $s_1 = \omega_o e^{j\frac{3\pi}{4}}$ and $s_2 = \omega_o e^{-j\frac{3\pi}{4}}$, then the coefficients k_p and k_i are:

$$k_p = \frac{C}{2\times\left(1+\sqrt{2}\right)\times\tau_3} \tag{30}$$

$$k_i = \frac{C}{2\times\left(1+\sqrt{2}\right)^3\times\tau_3^2} \tag{31}$$

If the load resistor is considered (R), then the coefficients become [12]:

$$k_i = \frac{\left(T+\tau_1\right)^3}{T^2\tau_1^2\left(1+\sqrt{2}\right)^3 R_L} \tag{32}$$

$$k_p = \frac{1}{R_L}\left(\frac{\left(T+\tau_1\right)^2}{\left(1+\sqrt{2}\right)T\tau_1}-1\right) \tag{33}$$

where $T = R_L \times C$.

IV. Simulation Results

To validate the above study, the Simetrix 5.3 software platform has been used to simulate the proposed topology (Fig. 9). The values of the elements have been very conservative chosen as: V_b =12 V, L = 100 µH, r_L = 0.1 Ω, C = 100 µF, R_L = 100 Ω, and the switching frequency of f_s = 100 kHz. The diode used (10CTQ150) presented a voltage drop of V_d = 0.7 V with slight variation depending on output power and the switch elements (IRF613) was considered as r_{dson} = 50 mΩ.

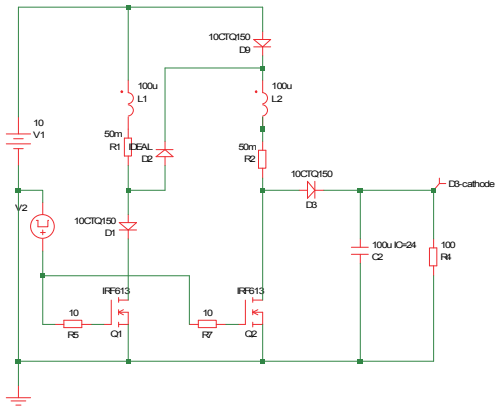

Fig. 9 Simulation model

The simulation was performed for few values of the duty cycle; the output voltage has been determined in order to validate the boost ratio M. Figure 10 shows the output voltage and the voltages across the two inductors for duty cycle 0.5 and 0.8.

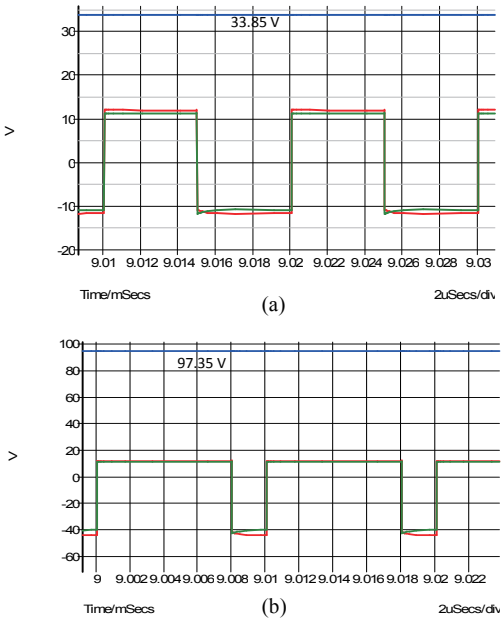

Fig. 10 Main voltages: a) δ = 0.5; b) δ = 0.8

Table I presents the parameters results for various values for the duty cycle from which the boost ratio has been determined. The parameter M_i is the ideal value for two inductors model, M_c is the corrected boost factor considering the losses and V_o is the output voltage determined via simulation.

TABLE I
BOOST RATIO VS DUTY CYCLE

δ (%)	V_o (V)	V_o/V_b	M_c	M_i
50	33.85	2.821	2.897	3.000
60	45.05	3.754	3,879	4.000
75	76.85	6.404	6.697	7.000
80	103.4	8.617	8.918	9.000
85	129.4	10.78	11.76	12.33
90	118.5	9.875	10.87	19.00

The results show a fairly good validation of equation (6). The reason for the error consists in the influence of the transients and the difference in inductance currents. Figure 11 shows the inductor waveform deviation due to transients. Figure 12 shows the inductor currents difference; this difference is attributed to the diode series with the second inductor.

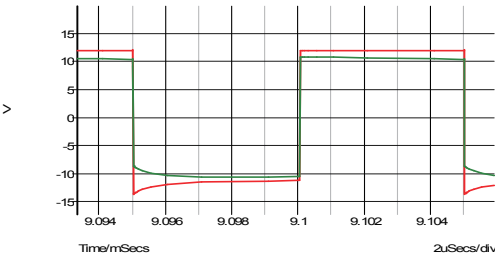

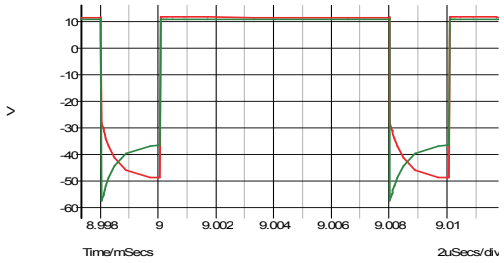

Fig. 11 Inductor voltages transient influence: a) δ = 0.5; b) δ = 0.8

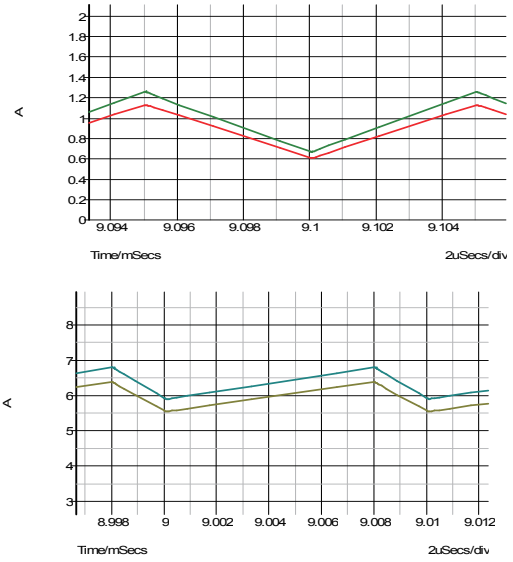

Fig. 12 Inductor currents difference: a) δ = 0.5; b) δ = 0.8

V. Experimental Results

An experimental model has been built. Fig. 10 shows the experimental set. The practical model was supplied from a battery of V_b = 12.75 V (no load). The other parameters of the experiment were: the inductors L_1 = 87.8 µH, L2 = 85.9 µH (measured at 100 kHz) both with internal resistance of r_L = 0.085 Ω, the load 680 Ω, the smoothing capacitor 100 µF, IRF613 as switching transistors, 10 CTQ150 as diodes and 100 kHz as switching frequency.

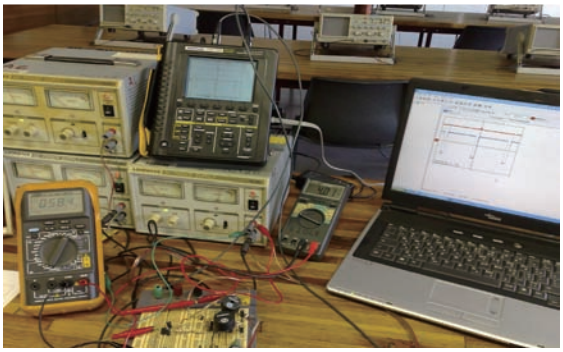

Fig. 10 Experimental set-up

For a duty cycle of 80 percentages, the output voltage was 112.4 V for the given 12.6 V input voltage (V_b). Fig. 11 shows The output voltage (orange), the input voltage (green), the drain voltage of switch S_2 (pink) and the drain voltage of switch S_1 (blue).

Fig. 12 shows the voltage across the inductor L_1 (orange) and the drain voltage of switch S_1.

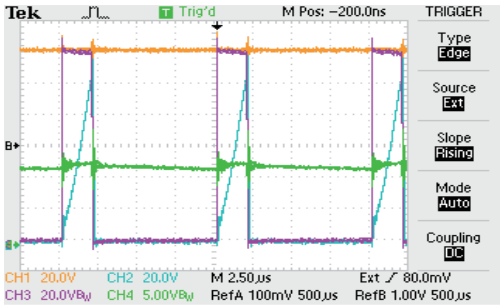

Fig. 11 Experimental graphs

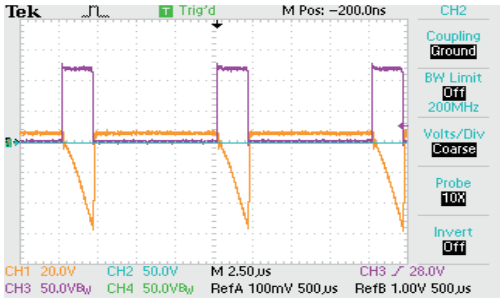

Fig. 12 Inductor voltage across L_1

Table II presents the boost factor for few values of the duty cycle as determined experimentally.

TABLE I
BOOST RATIO VS DUTY CYCLE

δ (%)	V_o (V)	V_b (V)	M
50	35.6	12.65	2.814
60	48.9	12.65	3,865
70	62.9	12.64	4.976
75	83.4	12.63	6.603
80	112.4	12.62	8.908
85	139.5	12.61	11.06
90	126.9	12.60	10.07

Figure 13 shows the currents through the two inductors. As predicted and shown via simulation, the currents through inductors are not equal.

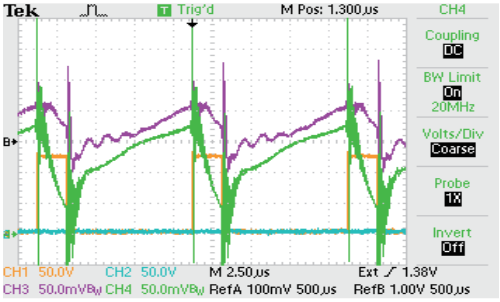

Fig. 13 Inductor voltage across L_1

VI. Conclusion

This paper presents a variation of the classical boost converter with the aim of improving the boost factor. The general idea is to charge parallel the inductors and transfer serially to the output increasing the boost ratio. The influence of the losses is presented is concluded that this application is not effective for more than two inductors.

The performances of this novel boost converter are validated via simulation and experimental model.

References

[1] J.A. Morales-Saldaña, et al, Modeling of a Cascade Boost Converter with Single Switch, *The 32nd Annual Conference of the IEEE Industrial Electronics Society*, 2006

[2] W. Lee, et al, "Interleaved ZVT Boost Converters with Winding Inductors and Built-In LC Low-Pass Output Filter Suitable for Distributed Fuel Cell Generation System", *38th IEEE Power Electronics Specialists Conference*, 2007

[3] H.C. Iu, "Experimantal Study of Instabilities in Two paralle-Connected Boost Converter under Current Mode Control", *11th European Conference on Power Electronics and Applications*. 2005

[4] M. Veerachary, "General Rules for Signal Flow Graph Modeling and Analysis of DC-DC Converters", *IEEE Trans. On Aerospace and Electronics Systems*, Vol. 40, No. 1, pp. 259-271, Jan. 2004

[5] N. Vazquez, L. Estrada, C. Hernandez and E. Rodriguez, « The Tapped-Inductor Boost Converter", *IEEE International Conference on Industrial Electronics (ISIE)*, 2007

[6] Y. Bercovich, B. Axelrod, S. Tapuci and A. Ioinovici, "A Family of Four-Quadrant DC-DC Converters", *38th IEEE Power Electronics Specialists Conference*, 2007

[7] G. Thiele and E. Bayer, Voltage Doubler/Tripler Current-Mode Charge Pump Topology with Simple "Gear Box", *38th IEEE Power Electronics Specialists Conference*, 2007

[8] B.S. Min, N.J Park and D.S. Hyun, "A Novel Current Sharing Technique for Interleaved Boost Converter", *38th IEEE Power Electronics Specialists Conference*, 2007

[9] I. Batarseh, *Power Electronics Circuits*, John Wiley & Sons, Inc. 2004, pp. 189-199

[10] Q. Zhou, Y. Huang, F. Zeng and Q-S. Chen, "Dynamic analysis of DC-DC Converter Based on Its Nonlinear Characteristics", *The 32nd Annual Conference of the IEEE Industrial Electronics Society*, 2006

[11] S.J. Mason, "Feedback Theory-Some Property of Signal Flow Graphs", Proceeding IRE, Vol. 41, No. 9, pp. 1144-1156, Sept. 1953